

Backward Couplers Waveguide Orthomode Transducer for 84-116 GHz

Alessandro Navarrini^{1,*}, and Renzo Nesti²

¹*INAF-Cagliari Astronomy Observatory, Cagliari, Italy*

²*INAF-Arcetri Astrophysical Observatory, Florence, Italy*

* Contact: navarrin@ca.astro.it, phone +39-070-711 80 218

Abstract— We describe the design, construction, and performance of a waveguide Orthomode Transducer (OMT) for the 3 mm band (84-116 GHz.) The OMT is based on a symmetric backward coupling structure and has a square waveguide input port (2.54 mm x 2.54 mm) and two single-mode waveguide outputs: a standard WR10 rectangular waveguide (2.54 mm x 1.27 mm,) and an oval waveguide with full-radius corners. The reverse coupling structure is located in the common square waveguide arm and splits one polarization signal in two opposite rectangular waveguide sidearms using broadband -3 dB E-plane branch-line hybrid couplers.

The device was optimized using a commercial 3D electromagnetic simulator.

The OMT consists of two mechanical blocks fabricated in split-block configuration using conventional CNC milling machine.

From 84 to 116 GHz the measured input reflection coefficient was less than -17 dB, the isolation between the outputs was less than -50 dB, the cross polarization was less than -30 dB, and the transmission was larger than -0.35 dB at room temperature for both polarization channels.

The device is suitable for scaling to higher frequency.

I. INTRODUCTION

An OMT is a diplexer that separates two orthogonal linearly polarized signals within the same frequency band. A common way to separate orthogonal polarizations is to use a wire-grid that directs the orthogonal signals to two independent feedhorns. A waveguide OMT is a useful alternative to the grid because it can be linked to a single feedhorn and fits more easily in a cooled receiver.

An OMT has three physical ports but exhibits properties of a four-port device, because the input common port, usually a waveguide with a square or circular cross-section, provides two electrical ports that correspond to the independent orthogonal polarized signals. In modern radio-astronomy receivers, requirements of the OMT are a high cross-polarization discrimination between the orthogonal signals (better than ~40 dB,) low insertion loss (a few tenths of a dB,) and a good match of all electrical ports (return loss above ~20 dB) over bandwidths of 30% or wider.

Several asymmetric OMTs have been designed with performance limited to a fractional bandwidth of 10-20% by

the excitation of higher order modes in the common port. Highly symmetric structures are required to achieve a waveguide OMT with bandwidth of 25 to 40%.

Because the small dimensions and tight tolerances pose a significant challenge for the fabrication and assembly of the parts [1] only few broadband OMT designs have been demonstrated to work well at mm-wavelengths. One such design is based on the two-fold symmetric junction introduced by Bøifot [2] and uses a thin metallic septum centered in a square waveguide common port and capacitive compensation pins located at the entrance of two waveguide sidearms. The broadband OMTs adopted for the 84-116 GHz and 211-275 GHz bands [3] of ALMA (Atacama Large Millimeter Array) are variants of the Bøifot design. Other Bøifot style OMT designs with a thicker septum have also been proposed; here, the pins are eliminated in favour of short capacitive steps [4] [5] or standard multistep transitions on the sidearms [6]. Although in these cases the construction of the blocks is simplified, the precise alignment of the septum inside the waveguide remains critical.

An alternative to the Bøifot design based on a four-fold symmetric turnstile junction OMT was developed for the 200-270 GHz band [7]-[8] of CARMA (Combined Array for Research in Millimeter Wave Astronomy.) A similar OMT design was also developed to cover the band 75-110 GHz [9]. An advantage of the turnstile junction design is that neither the pins nor the septum of the Bøifot junction are required to achieve polarization separation and low VSWR over a wide bandwidth, which makes this OMT easy to assemble; a disadvantage of such design is that the OMT fabrication requires that the symmetric structure is either split in four blocks rather than the two of the Bøifot design (so adding mechanical complexity with potential misalignment problems between the four quarters,) or manufactured by electroforming techniques, where copper is grown onto a gold-plated aluminum mandrel that is subsequently dissolved. However, one of the drawbacks of the electroforming technique is that complex mandrels are difficult to fabricate with high mechanical accuracy, therefore limiting the maximum achievable operational frequency [10].

An OMT design that can be fabricated with a standard end-mill by machining only two mechanical blocks and that has neither pins nor metallic septum, is based on a symmetric double ridged design. This type of OMT was developed at the ATNF (Australia Telescope National Facility) for the 77-117 GHz band [11] and was also adopted at NAOJ (National Astronomical Observatory of Japan) for the ALMA 125-163 GHz band [12]. The OMT consists of a square to double ridged guide transition followed by a junction of two sidearms with the central guide (similar to the Bøifot design.) A disadvantage of this OMT is the complexity of machining with high accuracy the narrow stepped double ridge centered in the middle of the square waveguide input (typical ridge widths are between $0.1 a$ and $0.15 a$, where a is the waveguide width.)

Recently, a novel OMT architecture based on a backward coupling structure was developed for operation at 32 GHz (Ka band) [13]. The OMT is based on a single-side branch-line coupling structure whose asymmetry limits the operation bandwidth of the device to $\sim 10\%$.

Here, we present the design, construction, and test results of an OMT with architecture similar to the one presented in [13], but where the single-side branch-line backward coupler is replaced by a broadband *symmetric* dual-side backward coupler. Our OMT covers the 84-116 GHz band (32% fractional bandwidth) and has excellent performance. The device is easy to machine and assemble; it was fabricated in two mechanical blocks by standard numerically controlled end-mill. The performance of the OMT is robust against small changes of the geometry associated with mechanical tolerances. The device is suitable for scaling to higher frequencies.

II. SYMMETRIC REVERSE COUPLING STRUCTURE

The network representation of an ideal backward coupling structure based on a 90° hybrid coupler is shown in Fig. 1. The input signal at port 1 is split at -3 dB with 90° phase difference between the hybrid *through output port* (port 4) and *coupled output port* (port 3.) Both outputs are terminated with equal reactive loads. Therefore, after a total reflection at the outputs, the two signals are sent backward and recombined in-phase at port 2 and out-of-phase at port 1 (destructive interference.) The net effect is that the input signal at port 1 is fully coupled to port 2, i.e. with reverse direction. This may be thought of as a 0 dB backward coupler.

A backward coupler that carries two orthogonal polarization signals Pol 1 and Pol 2 at its input (for example a square waveguide port) can also be used as a polarization splitter, i.e. as an OMT. A schematic representation of an ideal OMT based on a reverse coupling structure is shown in Fig. 2. Here, Pol 1 is fully transmitted from input port 1 to output port 4 and therefore does not couple through the hybrid to ports 2 and 3 (straight coupling.) Pol 2 signal couples through the hybrid and sees reactive loads at both its terminations, ports 3 and 4. Therefore, after total reflection at those ports, Pol 2 signal is fully transmitted in backward

direction to port 2. The schematic network for Pol 2 signal is the same as the one depicted in Fig. 1. In summary, the schematic of Fig. 2 represents an OMT with forward coupling for Pol 1 and backward coupling for Pol 2. We note that the OMT has three physical ports (1, 2 and 4) and four electrical ports because two orthogonal modes propagate through the input port 1.

An OMT based on a *asymmetric* waveguide backward coupling structure, as the one schematized in Fig. 2, was described by Peverini in [13]. There, a square waveguide input propagates the two orthogonal polarization states. A 0 dB backward coupler consisting of the square waveguide parallel to a *single* rectangular waveguide was used; while Pol 1 is directly coupled through a square-to-rectangular waveguide multistep transition, the coupling of Pol 2 signal between the parallel waveguides was achieved using four apertures (slots) in the rectangular waveguides E-plane; the two forward waveguide ports of the hybrid coupler were terminated with

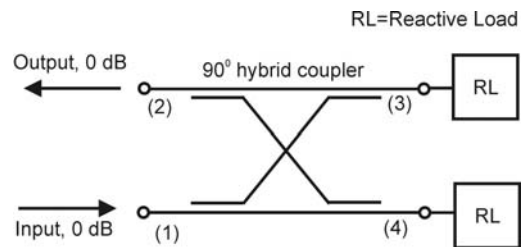


Fig. 1. Schematic representation of a backward coupling structure consisting of a 90° hybrid coupler with output ports terminated with equal reactive loads.

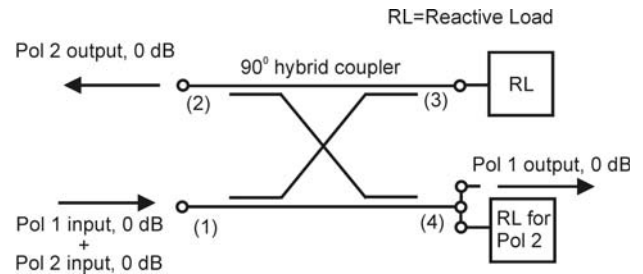


Fig. 2. Schematic representation of an ideal polarization splitting network (OMT) with forward coupling of Pol 1 from ports 1 to 4 and backward coupling of Pol 2 from port 1 to port 2. The structure consists of a 90° hybrid coupler with reactively loaded outputs.

reactive loads for Pol 2. The asymmetry of the reverse coupling structure presented in [13] limits the bandwidth of such device to $\sim 10\%$ due to the excitation of higher order modes in the square waveguide.

The network representation of the *symmetric* backward coupling structure used in our OMT is shown in Fig. 3. Here, Pol 1 and Pol 2 propagate through a common input port. Pol 1 input signal is fully coupled to the straight output port 4. Pol 2 input signal at port 1 is equally split between two 90° hybrid couplers whose output ports (4, 5, and 6) are

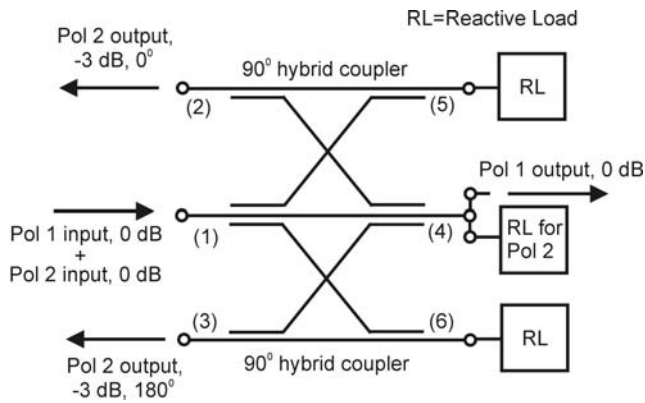


Fig. 3. Schematic representation of the ideal polarization splitting network (OMT) with forward coupling of Pol 1 from ports 1 to 4 and symmetric -3 dB backward coupling of Pol 2 from port 1 to ports 2 and 3. The structure consists of two 90° hybrid couplers with reactively loaded outputs. Port 1 is in common to the two hybrids. Signals at ports 2 and 3 are 180° out-of-phase.

terminated with reactive loads; the input port is in common with both hybrids. Pol 2 signal is coupled at -3 dB to output ports 2 and 3 with a phase difference of 180°.

III. POLARIZATION SPLITTING BACKWARD COUPLERS

A 3D view of the symmetric waveguide backward coupling structure used in our OMT, equivalent to the network of Fig. 3, is illustrated in Fig. 4. This consists essentially of: *a*) a square common waveguide input that goes through a two-section transformer to a reduced height rectangular waveguide; *b*) two 90° hybrid waveguide couplers on the sidearms; *c*) a reactively loaded termination at each hybrid coupled port.

The square waveguide input (2.54×2.54 mm²) propagates two orthogonal linear polarized signals Pol 1 and Pol 2 associated, respectively, with the TE₁₀ and TE₀₁ fundamental modes, when the wavelength is below the cut-off value $\lambda_c(\text{TE}_{10}) = 2a = 5.08$ mm (frequencies above $\nu_c = 59.01$ GHz.) Besides the fundamental modes, higher order modes can propagate in the square waveguide in the 84-116 GHz frequency band of interest. These are the TE₁₁ and TM₁₁ that have the same cut-off frequency of $\nu_c = 83.46$ GHz. In theory, these modes can be excited by the discontinuity created by the apertures (slots) of the sidearms. However, their excitation can be avoided as long as the two-fold symmetry of the structure is maintained. The adopted symmetry enables broadband operation allowing to achieve a relative bandwidth for the device larger than ~30 %.

The symmetric coupling structure in the common square waveguide arm splits with opposite phases the incoming Pol 2 signal in the two rectangular waveguide sidearms. Signal coupling to each sidearm is obtained with a broadband 90° hybrid coupler realized as a 3-dB E-plane branch-line coupling structure with four branches. The four 0.45 mm wide apertures through the broad walls of the waveguide sidearms are equally spaced of 0.34 mm (see details in Fig. 5.) The branches have a length of 0.75 mm. The through port and the coupled port of each hybrid are terminated with

reactive loads for Pol 2. In the common arm, the reactive load is provided by a two-section transformer polarization discriminator that reflects back all Pol 2 power in the frequency range of design, 84-116 GHz. Indeed, the output rectangular waveguide section of such transformer has size 2.54×1.22 mm² that cuts off the propagation of the TE₀₁ mode associated with Pol 2 to frequencies above $\nu_c(\text{TE}_{01}) = 122.87$ GHz, outside our operating range. On the other hand, the orthogonal polarization, Pol 1, is relatively unaffected by the presence of both the branch-line apertures in the two sidearms and of the common arm two-section transformer. Each section of such transformer is approximately a quarter wavelength long. Therefore, Pol 1 is well matched to the output and is fully coupled to the fundamental TE₁₀ mode of the rectangular waveguide output in the common arm (forward coupling.)

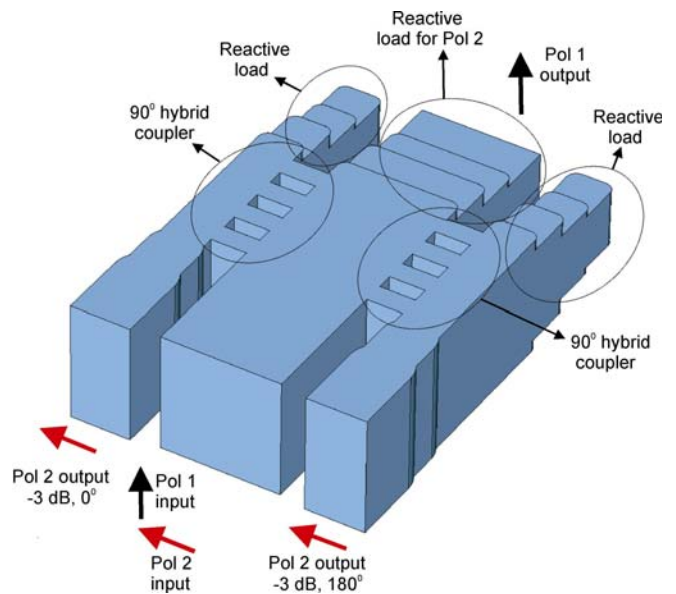


Fig. 4. Internal view of the symmetric dual-side backward coupler of our OMT with input square waveguide in common with two -3 dB E-plane branch-line coupling structures terminated with reactive loads for Pol 2. The device has four physical ports and five electrical ports.

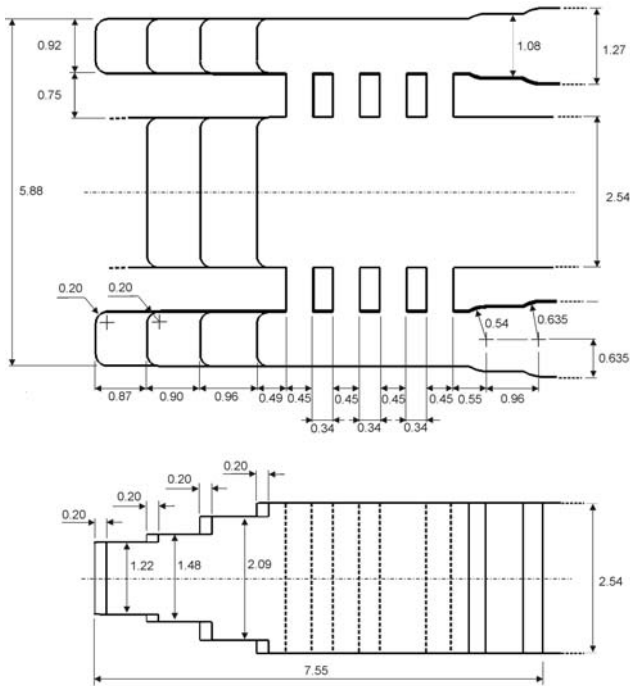


Fig. 5. Cutout views with dimensions (in mm) of the symmetric backward couplers of Fig. 4. The structure was optimized for operation in the 84-116 GHz band.

In the rectangular waveguide sidearms, the reactive loads for Pol 2 are provided by a short circuited three-step H-plane discontinuity (two transformer sections.) The transformer sections have the same physical length and height in the sidearms and in the common arm to guarantee that Pol 2 sees the same impedance when looking toward the through and coupled ports of the hybrids. This allows the split Pol 2 signals, which are reflected backward by the reactive loads, to recombine out-of-phase in the common arm (thus providing a destructive interference with low reflection at the common port) and in-phase in the two opposite sidearms. The constructive interference of the backward waves provides a coupling of -3 dB to each rectangular output port. Pol 2 signals at these two ports are 180° out-of-phase to each other because the E-field signal at the common square input couples to the two sidearm hybrids in opposite directions. The rectangular waveguide sidearms have a reduced height in the coupling section of the hybrids (0.92 mm rather than full 1.27 mm) in order to increase the bandwidth of the device.

The waveguide steps of the two-section transformers have round corners (radius 0.20 mm) to allow easy machining of the parts with an end-mill. Each reduced-height rectangular waveguide sidearm carrying the reverse-coupled -3 dB Pol 2 signal is transformed to standard WR10 full-height 2.54×1.27 mm² waveguide at the hybrid signal output. This is accomplished by a single-section quarter-wave transformer (0.96 mm long.) The use of the standard WR10 full-height waveguide reduces the insertion loss of the single-mode transmission line to its minimum possible value across the band of interest. The steps of the transformers are rounded as

they would be if machined with an end-mill of diameter equal to the height of the waveguide transformers (1.08 mm.)

The electrical performance of the structure of Figs. 4-5 was optimized using the commercial electromagnetic simulator CST Microwave Studio³ based on the finite integration technique. The parameters that were varied in the optimization were the number of branches of the hybrid couplers, their lengths, widths, spacings, the dimensions of the two-section transformers in the main and sidearms, the position of the sidearm short-circuits, the size of the common square waveguide and rectangular waveguide sidearms and of their single-section output transformer. It was found that an increase in the number of branches of each hybrid (a minimum of two is required) would increase the bandwidth of the device (but the branch length would have to be decreased.) However, an optimum number of branches was found to be four, beyond which the performance of the device would only have very little improvement but the mechanical fabrication would become more difficult. Also, we found that the widths and the spacing of the four branches could be chosen to be all equal (rather than with different values) without any degradation of the electrical performance. For the reactive load sections, we found that the optimum number of steps was three (two transformer sections.)

As expected, the performance of the two polarization channels are tightly connected. Indeed, we found using simulation that improving the performance of one polarization channel would typically degrade the performance of the other. For example, the heights and lengths of the waveguides of the two-section transformer in the common arm that optimizes the transmission of Pol 1 does not provide the optimum transmission for the backward coupled Pol 2. A trade-off was found to provide good performance for both polarization channels. An important aspect of the device in Figs. 4-5 is that its performance has proven robust against small changes in the geometry associated with the mechanical tolerances.

Fig. 6 shows the final simulation results for the reflected amplitude of the two independent fundamental modes TE₁₀ and TE₀₁ at the square waveguide input of the device illustrated in Fig. 4 (the three rectangular output ports are terminated by matched loads.) In the graph, vertical lines denote the nominal band edges at 84 and 116 GHz. The reflection coefficient is below -20 dB for both polarizations over the entire band of interest.

IV. OMT DESIGN

Our OMT basically consists of a dual-side backward coupler, two 180 deg and two 90 deg E-plane bends, an E-plane Y-junction power combiner, and a 90 deg E-plane rectangular-to-oval waveguide bend transition. Fig. 7 shows the complete OMT. The OMT single-mode waveguide outputs are a) an oval waveguide with full-radius corners (external cross-section dimensions of 2.78×1.27 mm²) for

³ CST Microwave Studio, Darmstadt, Germany.

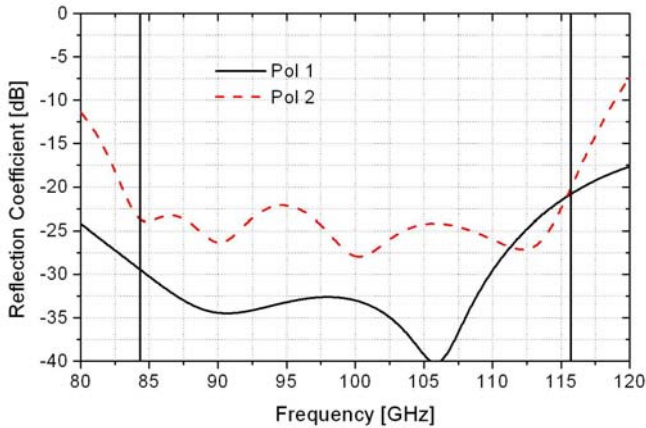


Fig. 6. Simulated reflection coefficient for the TE₁₀ (Pol 1) and TE₀₁ (Pol2) modes at the square waveguide input port of the device illustrated in Fig. 4.

Pol 1, and *b*) a standard WR10 rectangular waveguide for Pol 2. The OMT can be constructed in two mechanical blocks using conventional split-block techniques.

In the main arm, the signal associated with Pol 1, available at the output of the two-section quarter-wave transformer, travels through the E-plane 90 deg bend transition that brings out, orthogonal to the main arm, the oval cross section port; the oval waveguide is easy to machine with an end-mill and can be attached to a standard WR10 waveguide producing a

waveguide with the oval waveguide terminated into a matched load. The reflection coefficient is below -18 dB across the band of interest; the reflection increases at the higher frequencies. Slightly different geometries of the 90 deg rectangular-to-oval bend transition exist that have better performance than the one shown in Fig. 9. However, it was found that the chosen bend configuration, when used in conjunction with an optimum 1.0 mm long rectangular waveguide section connecting the backward coupler common arm output to the 90 deg bend, gave the best results for the complete OMT illustrated in Fig. 7.

The two Pol 2 signals emerging backward with -3 dB power from the sidearms of the reverse-coupling structure travel through two symmetric waveguide paths whose symmetry plane is coincident with the E-plane of Pol 1 propagating in the common arm. Each Pol 2 signal travels through a 180 deg WR10 waveguide E-plane bend (3.93 mm inner diameter), a straight waveguide section (length of 9.5 mm), and a 90 deg waveguide E-plane bend (3.47 mm inner diameter); the two Pol 2 signals are recombined by an E-plane Y-junction power combiner with standard WR10 output whose axis is coincident with the one of the common waveguide.

Electromagnetic simulations show that the reflection coefficient of the 180 deg and 90 deg WR10 E-plane bends are, respectively, below -31 dB and -33 dB across the 84 to 116 GHz band.

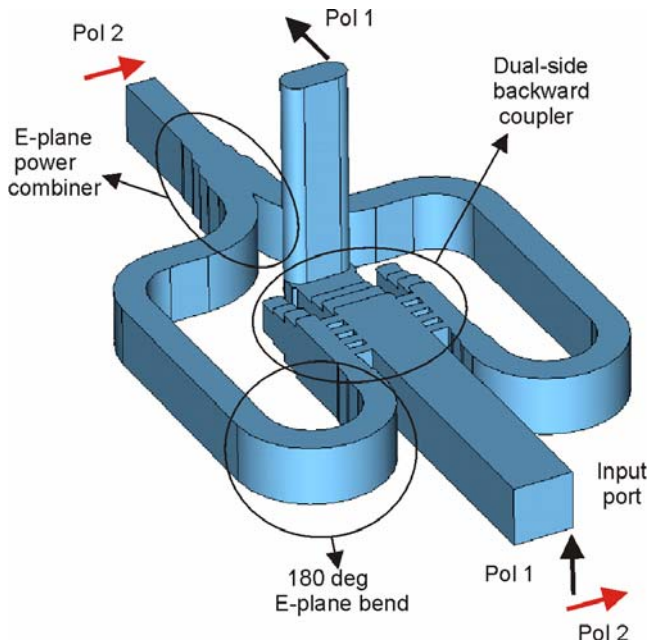


Fig. 7. Internal view of the OMT showing the polarization splitting dual-side backward coupler, the two 180 deg and 90 deg E-plane bends, the E-plane power combiner, and the 90 deg E-plane rectangular-to-oval bend transition.

negligible power reflection (return loss > 39 dB across 84-116 GHz.) Fig. 8 shows the internal details of such 90 deg rectangular-to-oval waveguide bend transition. The bend was based on a design by Narayanan [14] and the two steps are both below the split-block plane. Fig. 9 shows the simulation results for the reflection coefficient at the rectangular

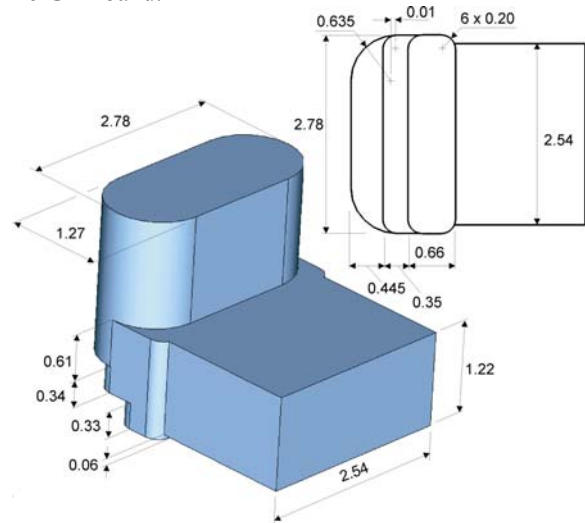


Fig. 8. Internal view of the 90 deg E-plane rectangular-to-oval waveguide bend transition. Dimensions are in mm.

The 180° out-of-phase Pol 2 signals at the backward coupler sidearms outputs are recombined using the E-plane Y-junction shown in Fig. 10. The combiner is based on a design by Kerr [15]. The steps of the three-section transformer are filleted so they can be machined with an end-mill of diameter equal to the WR10 waveguide height (1.27 mm.) The cusp at the junction of the curved arms is truncated at a width of 0.09 mm. Fig. 11 shows the simulated reflection coefficient at the common port when the two curved arms are terminated with matched loads. The reflection coefficient is below -33 dB from 84 to 116 GHz.

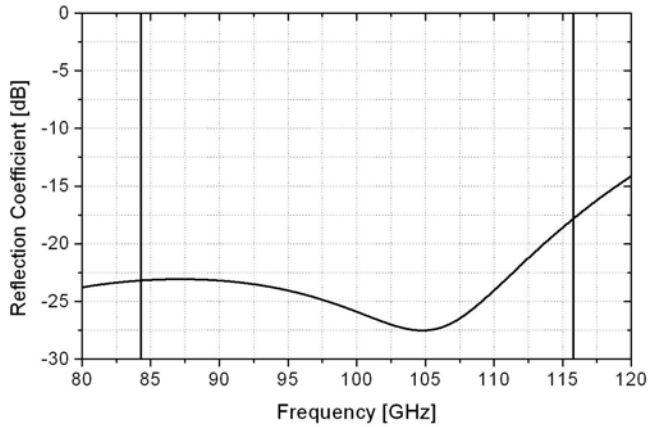


Fig. 9. Simulated reflection coefficient at the rectangular waveguide input of the 90 deg E-plane rectangular-to-oval waveguide bend transition of Fig. 8.

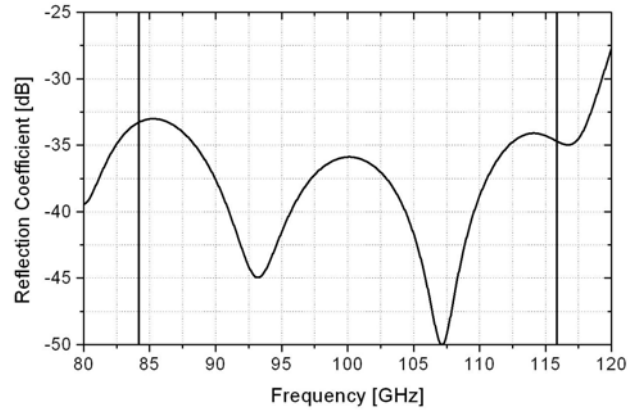


Fig. 11. Simulated reflection coefficient at the common waveguide port of the three-port device illustrated in Fig. 10.

The electrical lengths of the two sidearms between the Pol 2 backward coupler outputs and the power combiner inputs must be identical to guarantee that the signals recombine with the proper phase. An imbalance in the length of the sidearms caused by small fabrication error and mechanical tolerances determines a degradation of the OMT performance that may introduce a series of transmission resonances and an increase of the cross-polarization level.

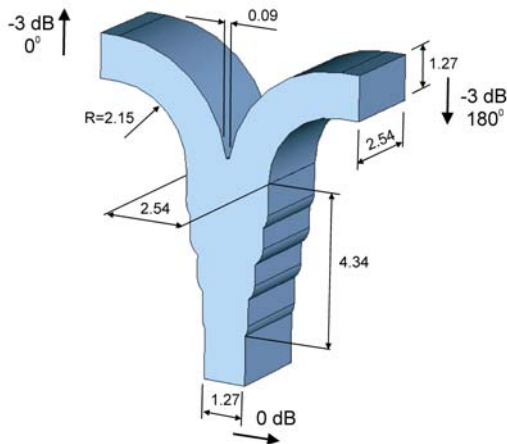


Fig. 10. Internal view of the E-plane Y-junction used to recombine the 180° out-of-phase signals associated to Pol 2 at the output of the dual-side backward coupler.

V. MECHANICAL DESIGN

The OMT is realized by splitting the structure of Fig. 7 along the E-plane of the side-coupled rectangular waveguides. Fig. 12 shows a photograph of the assembled OMT and of the two



Fig. 12. Photograph of the assembled OMT (left) showing the square waveguide input and the oval waveguide output. The external dimensions are $19 \times 30 \times 33 \text{ mm}^3$. Standard UG387 flanges are used at all ports. The two identical square-to-WR10 waveguide transitions used to test the OMT are shown on the right.

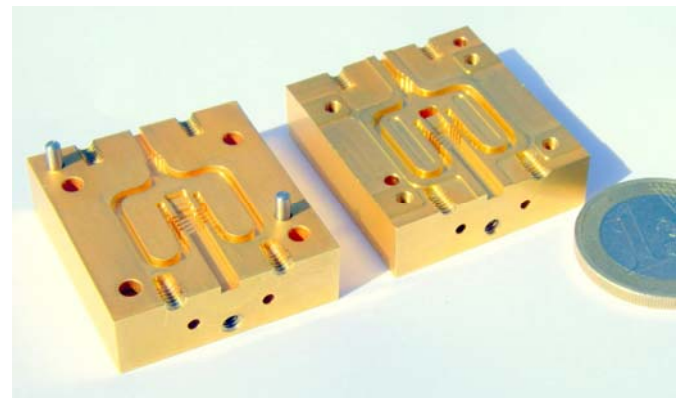


Fig. 13. Photograph of the two unassembled blocks of the OMT showing the internal waveguide circuitry.

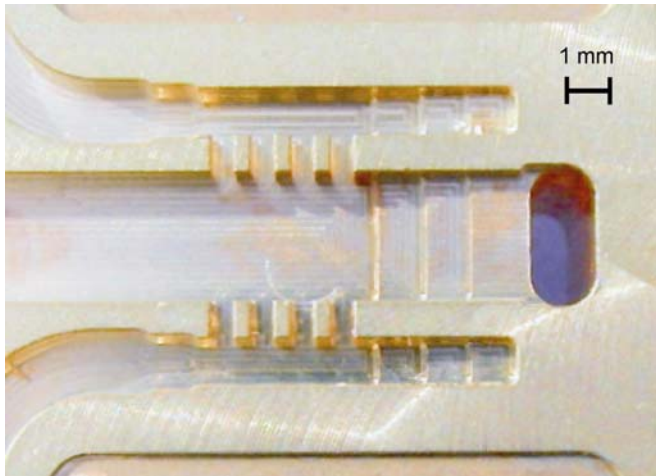


Fig. 14. Photograph of the internal details of one of the OMT blocks showing the dual-backward coupler waveguide circuitry and the three metal "teeth" between branch-line slots on both sidearms. The oval waveguide is also visible on the right.

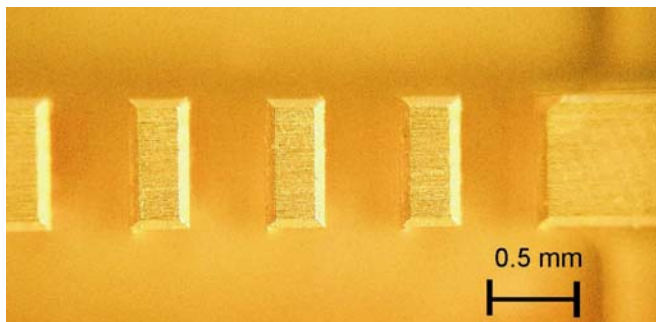


Fig. 15. Detail of the three metal "teeth" between branchline slots of one of the coupler sidearms.

identical square waveguide-to-rectangular waveguide transitions⁴ (linearly tapered 25.4 mm long 2.54×2.54 mm²-to-WR10 transitions) used to test it. The OMT accepts standard UG387 flanges at all ports. A photograph of the two unassembled OMT blocks and the internal mechanical details of one of the blocks are shown in Figs. 13-15. The blocks were fabricated in brass using a numerically controlled milling machine⁵. Then, they were gold plated by electrodepositing 1 μm thick pure Gold⁴ layer on top of a 0.2 μm thick Nickel interlayer. Unfortunately, two of the metal "teeth" between branch-line slots of the backward coupler were slightly damaged during the gold plating of the blocks. We expected that the small asymmetry of the structure resulting from the damaged teeth would degrade the cross-polarization properties of the OMT.

The blocks were aligned using two precision 2 mm diameter dowel pins. The tolerances for the waveguide channels in the two blocks and of the alignment between the blocks were specified at ± 10 μm. The blocks are bolted

together by four M2.5 stainless steel screws (type A2, grade 70.) Anti-coking recessed areas are used in one of the blocks: if we take the surface of the small area surrounding the waveguide channels as level of reference, all the remaining surface of the block is located 200 μm below that level except for four small areas around the screw holes located 10 μm below. The advantage of this design is that the flat surface of the mating block cannot be cocked by uneven tightening of the screws.

VI. EXPERIMENTAL RESULTS

The OMT was tested at IRAM (Institut de Radio Astronomie Millimétrique), Grenoble, France, using a millimeter-wave Vector Network Analyser [16] consisting of a HP8510C Network Analyser and millimeter-wave test set extensions. The millimeter-wave network analyser was calibrated at the WR10 rectangular waveguides at the outputs of the extension heads; we used one-port and two-port calibrations with WR10 calibration kit. The calibration procedure was used to remove systematic instrumental effects and to calibrate out the response of the instrument up to the chosen calibration planes. Additional measurement of two pairs of identical back-to-back WR10 waveguide-to-square waveguide transitions (shown in Fig. 12) allowed to calibrate out their individual effects and to derive the S-parameters of the OMT at the physical ports of the device. To obtain reproducible results, we took considerable care to minimize any movement of the cables and waveguides between calibration and tests and to align and tighten waveguide connections with a repeatable procedure.

A schematic of the Pol 2 transmission test setup is shown in Fig. 16. The square waveguide input of the OMT was attached to the WR10 waveguide port of the network analyser (port 1) through the WR10 waveguide-to-square waveguide transition. The transition was oriented to excite the Pol 2 in the OMT. The WR10 waveguide output of the OMT was attached to the second WR10 waveguide port of the analyser (port 2.) The oval waveguide of the OMT was terminated with a matched WR10 waveguide load. The transmission measurement of the other polarization channel was obtained with a setup similar to the one in Fig 15 but with WR10 waveguide-to-square waveguide transition rotated by 90 deg to excite Pol 1 at the OMT input and with waveguide matched load and second port of the analyser swapped at the OMT outputs. A photograph of the transmission test setup of Pol 1 is shown on Fig. 17. The measured transmissions of the OMT are illustrated in Fig. 18 for both polarization channels. Simulated results generated with CST Microwave Studio are shown for comparison. All simulations were performed with the full three-port model shown in Fig. 7, including the dual-side backward coupler, the 90 deg E-plane rectangular-to-oval waveguide bend transition, the 180 deg and 90 deg WR10 E-plane bends, the E-plane Y-junction power combiner, and all connecting waveguides. We assumed the conductor to be pure gold and used a gold conductivity of half its room temperature dc value $\sigma_{Au}=(4.26 \cdot 10^7)/2 \Omega^{-1} \text{m}^{-1}$. A Cartesian mesh was

² Custom Microwave Inc, Longmont, CO.

³ Fanuc Robodrill CNC milling machine.

⁴ The specification used for the Gold plating was MIL-G-45204C, Type III, Grade A, Class 0, 99.9% pure Gold.

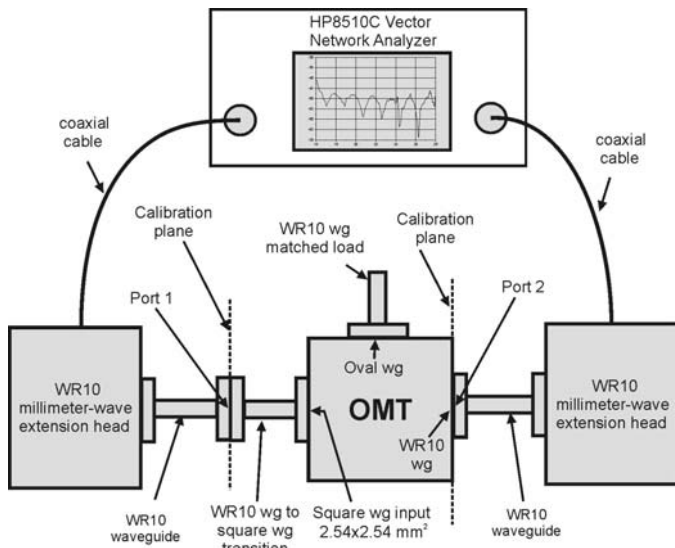


Fig. 16. S-parameter measurement of the OMT with the vector network analyser. The particular configuration refers to the transmission measurement of Pol 2.

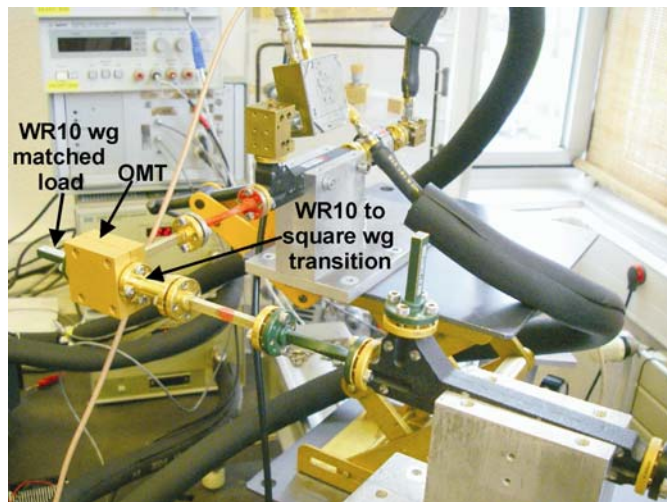


Fig. 17. Photo of the OMT during Pol 1 transmission measurement with the vector network analyser.

automatically generated and the time-domain solver calculated the broad-band response of the device in one simulation run. We set the parameter “lines per wavelength” to 15; this is the minimum number of mesh lines per wavelength in each coordinate direction for the shortest wavelength in the simulation.

The average measured transmission loss of the OMT is ~ 0.15 dB for Pol 1 (Fig. 18, top panel) and ~ 0.2 dB for Pol 2 (Fig. 18, bottom panel) similar in overall level to the value predicted by simulation. The insertion loss of the OMT is expected to decrease by a factor of ~ 3 when it is cooled to cryogenic temperatures [17]. Therefore, we expect a maximum insertion loss of below ~ 0.1 dB for both polarization channels when the OMT is operated at 4 K in front of SIS mixers or low noise amplifiers.

The physical length of the waveguide circuit of the OMT from its input to its output is approximately 22 mm for Pol 1 and 56 mm for Pol 2. The room temperature loss of a straight section of WR10 waveguide is in the range 0.05-0.07 dB/cm between 84-116 GHz [18]. For comparison, the loss of a 22 mm and of a 56 mm straight section of WR10 waveguide would be of the order of, respectively, 0.13 dB and 0.34 dB.

The reflection coefficient at the OMT input port was measured for both polarizations by terminating the OMT

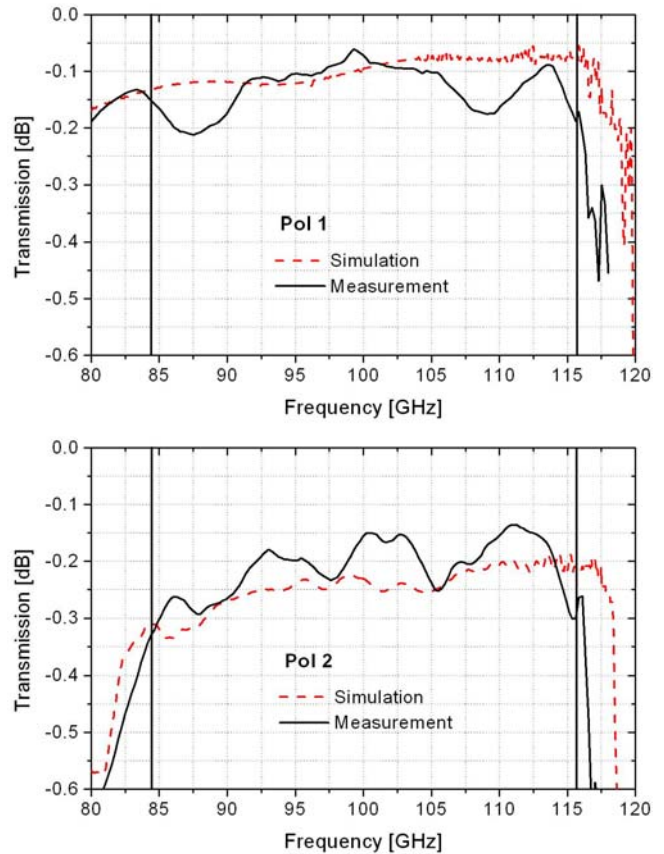


Fig. 18. Simulated and measured transmission of the OMT. *Top*): Pol 1; *Bottom*): Pol 2. The simulation (dashed lines) refers to the full three-port model shown in Fig. 7.

outputs with WR10 matched loads (one-port measurement.) The amplitude of the measured reflection is below -17 dB for both polarization channels (Fig. 19.)

An estimate of the OMT isolation was obtained by measuring the transmissions from the OMT output ports with its square waveguide input port open to free space. This gives an upper limit of the isolation of the device which should be measured, instead, using a matched load at the square waveguide input. An open square waveguide is, however, well matched to free space (reflection of the order of -20 dB.) The measured upper limit of the OMT isolation is below -50 dB across 84-116 GHz (Fig. 20.) There were no simulation results for the isolation since we used the perfectly symmetric model of Fig. 7, which produces perfect isolation.

The cross-polarization of the OMT, i.e. the signal from one polarization channel at the input that is coupled into the unwanted output channel, was estimated by measuring the transmission from the OMT oval waveguide to the OMT rectangular waveguide with the device input square waveguide terminated into a short circuit. The signal injected from the oval waveguide that is directly coupled into the rectangular waveguide when the wave travels through the dual-side coupling structure is extremely low, of the order of -50 dB (see isolation results.) Therefore, the wave from the OMT oval waveguide output is fully directed toward the

cross polarization level of the OMT, estimated with a short-circuit at its input, is below -30 dB across the band of interest (Fig. 21.) We note that this cross-polarization level of approximately -30 dB is consistent with the fact that the measured isolation upper limit of -50 dB is just -20 dB below

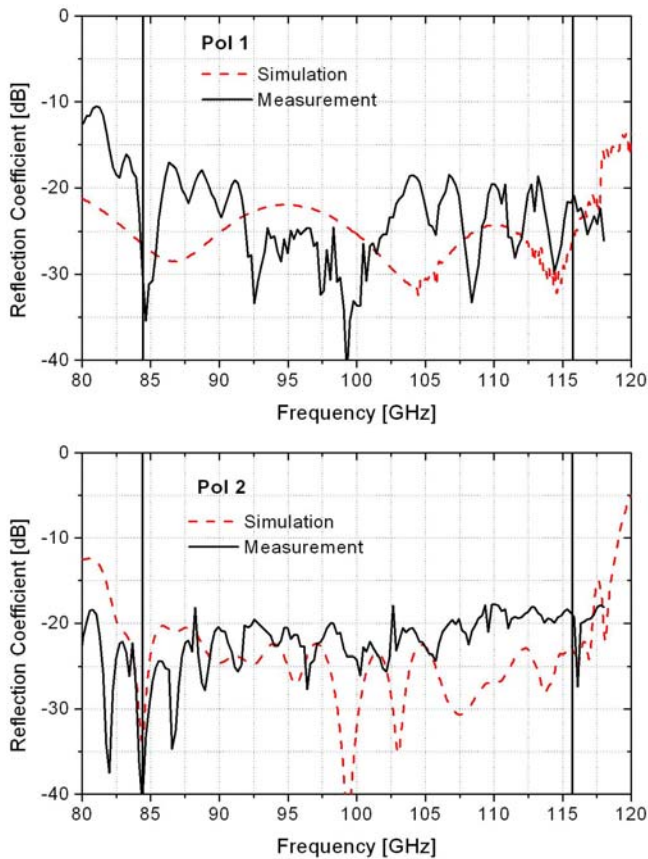


Fig. 19. Simulated and measured input reflection of the OMT. *Top*): Pol 1; *Bottom*): Pol 2. The simulation (dashed lines) refers to the full three-port model shown in Fig. 7.

short-circuited OMT input where it is reflected back with the same polarization; this is equivalent at injecting Pol 1 signal directly from the square waveguide input port (except for the small difference due to the device insertion loss.) Therefore, the signal level measured at the OMT rectangular port gives an estimate of the cross-polarization because it is equivalent at measuring the signal coupling between Pol 1 channel at the OMT common port and at the rectangular waveguide Pol 2 output. A direct cross-polarization measurement using a transmission setup similar to the one in Fig. 16, where the square waveguide-to-rectangular waveguide transition is rotated by 90 deg was also attempted, but it turned out not to be feasible because the cross-polarization of the waveguide transitions is larger than the one of the OMT. The measured

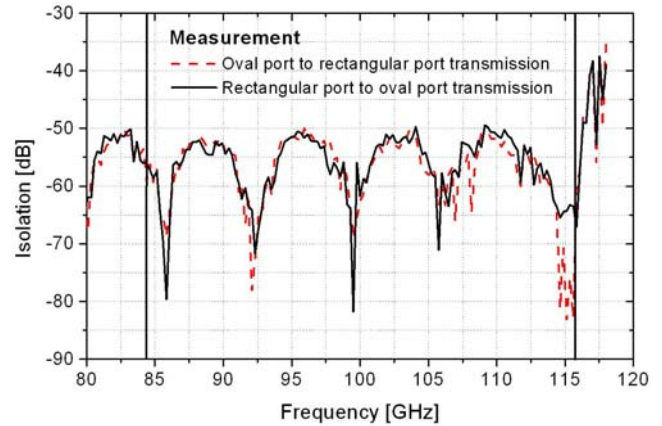


Fig. 20. Measured upper limit of the isolation: transmission between OMT output ports with square waveguide input open to free space.

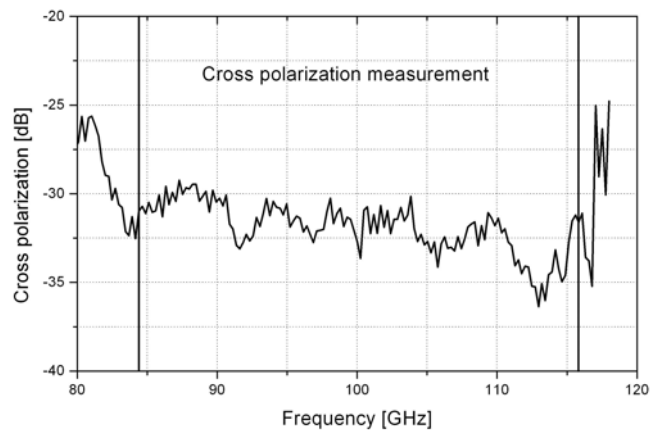


Fig. 21. Measure of cross-polarization: transmission between the oval waveguide port and the rectangular waveguide port of the OMT with short-circuited square waveguide input.

it, which would indeed correspond to the expected reflection from an open square waveguide. In this sense, the measured -50 dB upper limit of the isolation with the square waveguide terminated in free space would be explained by the combined -20 dB reflection at the open square waveguide transition cascaded with the -30 dB cross-polarization of the polarization splitting reverse-coupling structure.

We performed an electromagnetic simulation of the full OMT structure of Fig. 7 where small asymmetries were introduced in the geometry of the branch-line couplers, in order to evaluate the contribution to the overall OMT performance determined by the slightly damaged metal “teeth”. We found that these asymmetries do not change significantly the OMT transmission and input reflection, but can explain the overall level of measured OMT isolation and cross-polarization. Therefore, we would expect that an undamaged OMT of this

type would have superior isolation and cross-polarization performance than the one we tested.

CONCLUSIONS

We have presented the design, construction, and test of a 84-116 GHz waveguide OMT based on a symmetric reverse-coupling structure. The OMT was constructed as a split-block fabricated with a numerically controlled milling machine.

The OMT has state-of-the art performance: the measured room temperature insertion loss was less than 0.35 dB, the reflection was less than -17 dB, the isolation upper limit was less than -50 dB, and the cross-polarization level was estimated to be less than -30 dB for both polarization channels across the band 84-116 GHz. The predicted performance of the device, obtained with a 3D electromagnetic simulator, agree well with the experimental results.

The OMT is suitable for scaling to higher frequencies.

ACKNOWLEDGMENT

The authors would like to thank B. Lazareff, IRAM (Institut de RadioAstronomie Millimétrique,) Grenoble, France, for allowing testing of the OMT with the IRAM mm-wave Vector Network Analyser. The authors thank A.L. Fontana, IRAM, for her help during the measurements.

REFERENCES

- [1] A. Navarrini, R. L. Plambeck, "Orthomode Transducers for Millimeter Wavelengths," *URSI North American Radio Science Meeting*, Ottawa, Canada, Jul. 22-26, 2007.
- [9] A. M. Boïfot, E. Lier, T. Schaug-Petersen, "Simple and Broadband Orthomode Transducer," *Proceedings IEE*, vol. 137, n. 6, pp. 396-400.
- [10] E. J. Wollack and W. Grammer, "Symmetric Waveguide Orthomode Junctions," *Proceedings of the 14th International Symposium on Space Terahertz Technology*, Tucson, Arizona, Apr. 2003, pp 169-176.
- [11] G. Narayanan and N. Erickson, "Full-Waveguide Band Orthomode Transducer for the 3 mm and 1mm Bands," *Proceedings of the 14th International Symposium on Space Terahertz Technology*, Tucson, Arizona, Apr. 2003, pp 508-512.
- [12] R. Nesti, L. Cresci, P. Curioni, L. Lucci, G. M. Pancani, D. Panella, V. Natale, "22GHz Polarizer", Arcetri Astrophysical Observatory Technical Report. [Online]. Available: http://www.arcetri.astro.it/~nesti/pdfs/Faraday_22GHz_Polarizer.pdf
- [13] A. Navarrini and M. Carter, "Design of a Dual Polarization SIS Sideband Separating Receiver Based on Waveguide OMT for the 275-370 GHz Frequency Band," *Proceedings of the 14th International Symposium on Space Terahertz Technology*, Tucson, Arizona, Apr. 2003, pp 159-168.
- [14] A. Navarrini and R. L. Plambeck, "A Turnstile Junction Waveguide Orthomode Transducer," *IEEE Trans. Microwave Theory Tech.*, vol. 54, n. 1, pp. 272-277, Jan. 2006.
- [15] A. Navarrini A. Bolatto, R. L. Plambeck, "Test of 1 mm Band Turnstile Junction Waveguide Orthomode Transducer", *Proceedings of the 17th International Symposium on Space Terahertz Technology*, Paris, France, May 10-12, 2006.
- [16] G. Pisano, L. Pietranera, K. Isaak, L. Piccirillo, B. Johnson, B. Maffei, S. Melhuish, "A Broadband WR10 Turnstile Junction Orthomode Transducer," *IEEE Microwave and Wireless Components Letters*, vol. 17, n. 4, April 2007.
- [17] R. Banham, L. Lucci, V. Natale, R. Nesti, G. Pelosi, S. Selleri, G. Tofani, G. Valsecchi, "Electroformed Front-End at 100 GHz for Radio-Astronomical Applications," *Microwave Journal*, vol. 48, n. 8, pp. 112-122, August 2005.
- [18] G. G. Moorey, P. Axtens, M. Bowen, A. Dunning, R. Gough, G.R. Graves, H. Kanoniuk, "A 77-117 GHz cryogenically cooled receiver for radioastronomy," *Workshop in Applications of Radio Science (WARS2006)*, Leura, NSW, 15-17 Feb. 2006.
- [19] S. Asayama, "Double-Ridged Orthomode Transducer for ALMA Band 4 receiver," *Technical Memo of National Astronomical Observatory of Japan NINS*, 27 Feb. 2007.
- [20] O. A. Peverini, R. Tascone, G. Virone, A. Olivieri, R. Orta, "Orthomode Transducer for Millimeter-Wave Correlation Receivers," *IEEE Trans. Microwave Theory Tech.*, vol. 54, n. 5, May 2006.
- [21] G. Narayanan and N. Erickson, "A Novel Full Waveguide Band Orthomode Transducer," *Proceedings of the 13th International Symposium on Space Terahertz Technology*, Boston, Massachussets, Mar. 2002, pp 505-514.
- [22] A. R. Kerr, "Elements for E-plane Split-Blocks Waveguide Circuits," National Radio Astronomy Observatory, ALMA Memo No. 381, Jul. 2001.
- [23] F. Mattiocco and M. Carter, "80-360 GHz very wide band millimeter wave network analyser," *Int. J. of Infrared Millim. Waves*, vol. 16, n. 12, Dec. 1995, pp. 2249-2255.
- [24] E. J. Wollack, W. Grammer, J. Kingsley, "The Boïfot Orthomode Junction," ALMA Memo n. 425, May 2002.
- [25] A. F. Harvey "Microwave Engineering," Academic Press Inc. London, 1963, pp. 15.